GEOPHYSICAL RESEARCH LETTERS, VOL. 14, NO. 7, PAGES 749-752, JULY 1987

SHALLOW SEISMIC REFLECTION PROFILE OF THE MEERS FAULT, COMANCHE COUNTY, OKLAHOMA

Paul B. Myers, Richard D. Miller, and Don W. Steeples

Kansas Geological Survey, The University of Kansas

Abstract. A high-resolution seismic-reflection survey was conducted across the Meers fault in Comanche County, Oklahoma, in an attempt to determine the shallow structure associated with the fault zone. A downhole .50-caliber rifle was used as the seismic-energy source. Two 100-Hz geophones were connected in series at each receiver station. A 1.22-m station spacing was used for both source and receiver. Field recording parameters were set to optimize seismic reflections in the 40-150 millisecond range. A pre-analog-to-digital low-cut filter (24 dB/octave rolloff with -3 dB point of 220 Hz) resulted in dominant frequencies in excess of 150 Hz. Several interpretable reflection events between 40 and 120 msec on the processed seismic section provide a clear picture of the shallow structure. Reverse faulting is evident not only at the scarp itself but also on both the upthrown (north) and downthrown (south) portions of the line. This suggests the fault zone extends at least 180 m in both directions (north and south) from the scarp itself. Recent movement appears only to have occurred along the major fault associated with the scarp. The northern portion of the seismic line is characterized by gentle folding, which is not present on the southern portion.

Introduction

The Meers fault, located in southwestern Oklahoma, marks the southernmost boundary of the Frontal Fault System separating the Wichita uplift to the south and the Anadarko basin to the north (Figure 1). Until recently, the Meers fault was thought to have been tectonically stable since Permian time. Detailed geologic mapping resulted in the identification of a prominent scarp in Quaternary alluvium along the fault [Donovan et al., 1982; Gilbert, 1983a,b; Slemmons et al., 1985; Ramelli and Slemmons, 1986; Ramelli et al., 1987]. Trenching and carbon-14 dating at two locations revealed late Holocene high-angle reverse-slip deformation [Crone and Luza, 1986]. Maximum vertical displacement appears to be approximately 5 m [Ramelli and Slemmons, 1986; Ramelli et al., 1987]. In addition to vertical displacement, studies by Donovan et al. [1982], Butler [1980], McLean and Stearns [1983], Ramelli and Slemmons, [1986], and Ramelli et al., [1987] have demonstrated significant left-lateral strike-slip components of displacement associated with the Meers fault.

During mid-December 1986, the Kansas Geological Survey conducted a shallow high-resolution CDP seismic-reflection survey over the Meers fault in an attempt to achieve a better understanding of the shallow structure associated with the fault.

Paper number 7L7171.
0094-8276/87/007L-7171$03.00

Seismic Reflections and Fault Studies

High-resolution seismic reflection has only recently been introduced as a method for shallow (less than 100 m deep) fault delineation [Treadway et al., 1985; Miller and Steeples, 1986]. Fault detection at several hundred to several thousand meters depth is well established [Crone and Harding, 1984; Brewer, 1982]. Successful reflection surveys with shallow target depths (tens of meters) depend on recording frequencies of a few hundred Hz [Knapp and Steeples, 1986]. Raising the recorded frequencies will ultimately result in better resolution since resolution is directly proportional to frequency. Typically, the minimum resolvable bed is equal to 1/4 the wavelength of the dominant frequency [Widess, 1973]. Obtaining the desired high-frequency reflection energy ultimately lies in a careful choice of an energy source, proper field parameters, recording equipment, and processing techniques.

Field Methods and Data Processing

The high-resolution CDP seismic-reflection data were obtained directly over the Meers fault scarp (Figure 1). A modified .50-caliber rifle provided the seismic energy. The rifle was mounted on a steel plate with the barrel lowered approximately .6 m down a 4-cm-diameter augered hole. Lowering the barrel down a borehole diminishes the effects of the air-coupled wave and increases the overall amplitude of the recorded seismic energy [Steeples et al., 1987]. End-on source/receiver geometry was used in conjunction with two 100-Hz geophones connected in series at each receiving station. Receiver-station spacings were set at 1.2-m intervals providing 12-fold coverage every .6 m in the subsurface. The relatively close geophone spacing was used in an attempt to maintain continuity of reflectors across the fault zone. A walkaway-noise test was performed in order to determine the "optimum recording window" [Hunter et al., 1984]. The source spacing was twice the receiver spacing. Two shots were recorded individually at each shot station while incrementing the receivers one-receiver spacing for each shot. This resulted in two source-to-closest-receiver distances--the first at 29.3 m and the second at 30.5 m. This provided full subsurface coverage and cut the necessary number of shot holes augered by 50%.

An Input/Output, Inc. DHR 2400 seismic recording system was used to amplify, filter, convert from analog to digital, and record the data in the field. In order to increase the dominant frequencies recorded in the field, a severe analog low-cut filter with 24 dB/octave rolloff below the -3 dB point of 220 Hz was applied. As a result, recording frequencies and subsequent resolving power of the CDP section were increased.

Data processing was done on a Data General MV-20,000 computer at the Kansas Geological Survey (KGS). The software used to process the data was

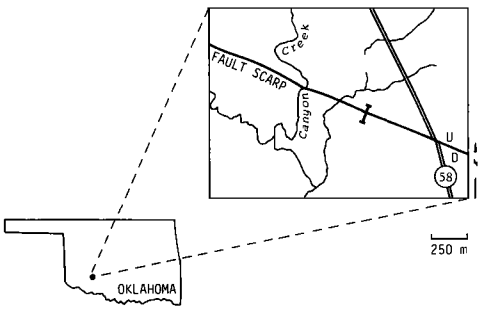

Fig. 1. Location map of the field site in Comanche County, Oklahoma. The seismic profile (indicated by the dark line) traversed the fault scarp approximately .5 km west of Highway 58.

the Seismic Processing Executive (SPEX) package by Sytech. The processing flow included elevation (static) corrections, muting, editing, CDP sorting, velocity analysis, surface-consistent statics, frequency spectral analysis, frequency filtering, and CDP stacking.

Results

Data quality of the .50-caliber seismic line remained good throughout the entire traverse of the fault. The three field records displayed in Figure 2 are from the upthrown side, directly over the scarp, and the downthrown side of the fault. All have high signal-to-noise ratios and seismic reflections, refractions, and air-coupled waves that can be identified directly on the field files from all three portions of the line. The surface waves arrived nearly simultaneously with the air-coupled waves. With the absence of identifiable reflection energy following the arrival of the air-coupled waves, the data were muted from the onset of the air-coupled waves to the end of the record. The first two arrivals on the field records (approximately 30 to 40 msec) are refractions and were muted during preliminary data processing. Most identifiable reflected energy arrives in a time window from approximately 50 to 120 msec, possessing frequencies from 100 to 250 Hz.

Reflections from the upthrown (north) side of the fault scarp do not display the classical hyperbolic moveout (Figure 2a). Amplitude, frequency, and wavelet character changes as well as undulations in the arrival pattern of individually reflected events are indicative of structurally complex areas. The first reflected energy arrives at approximately 50 msec on the record. The divergence of this event from the refracted arrivals above allowed complete removal of refracted energy from the data without sacrificing the shallow reflector. All the coherent seismic energy arriving after the 50-msec reflector and before the air-coupled waves appears to be reflections.

The fault can be detected directly between traces labeled 15 and 17 on a field record from over the major fault zone (Figure 2b). Similar to the upthrown side, the reflected energy first arrives at approximately 50 msec. The seismic energy does not appear to penetrate quite as deeply over the fault as on the flanks. This is probably due to the subsurface deformation within the fault zone. Orientation, frequency, and wavelet-character changes within individual reflectors again indicate deformational features along this portion of the line.

The reflected energy is significantly more coherent on the downthrown side of the fault scarp (Figure 2c). As on the upthrown side and directly over the scarp, most identifiably reflected energy arrives between approximately 50 and 120 msec. Seismic-energy penetration and signal-to-noise ratio appear to vary from file to file on the downthrown side. This is primarily due to the

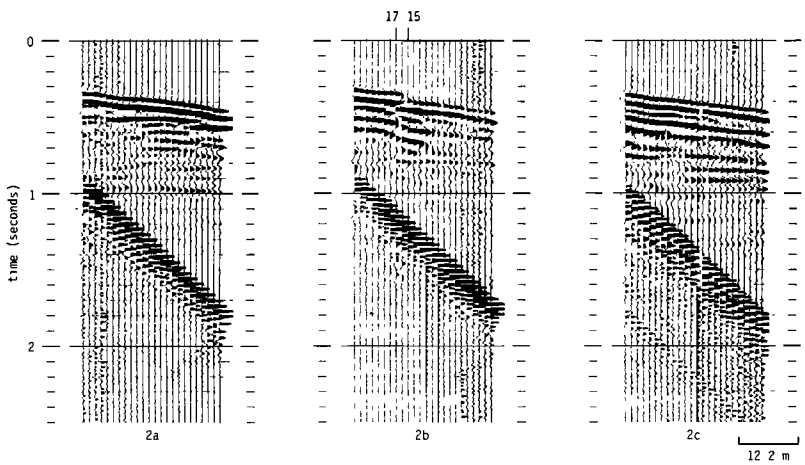

Fig. 2. Representative field files from the three major segments of the seismic profile. Refractions, reflections, and the air-coupled wave can be identified on all three files. (a) Representative field file from the upthrown (north) portion of the major fault associated with the scarp. The reflected events indicate complex orientations of reflecting horizons. (b) Representative field file directly over the fault. The offset visible between traces 15 and 17 is interpreted to be a result of the major faulting associated with the scarp. (c) Representative field file from the downthrown (south) portion of the major faulting. Coherency of reflected energy increased on the downthrown side.

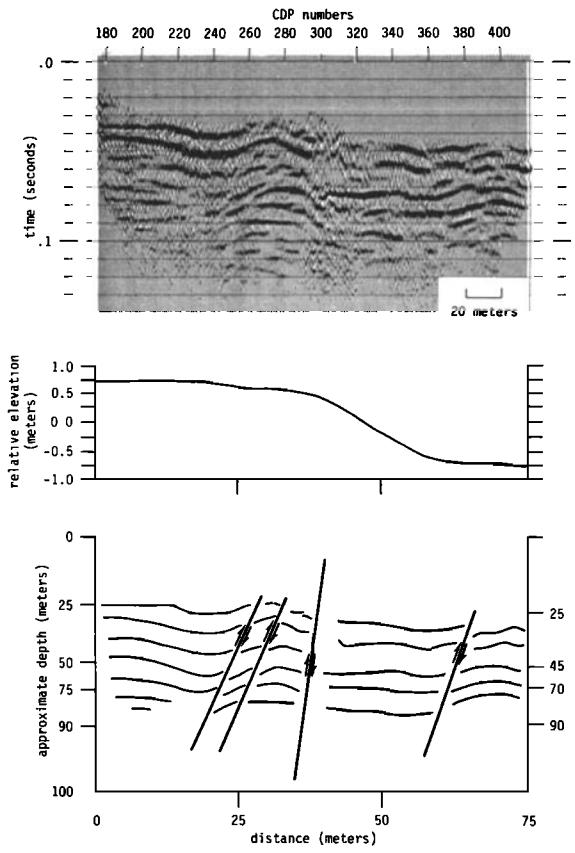

Fig. 3. Processed and stacked 12-fold CDP seismic section, relative-elevation diagram, and interpretive line drawing are plotted with the same horizontal scale. The major fault associated with the scarp is located between CDP 295 and 315. Additional faulting can be seen at approximately CDP 268, 283, and 384. The approximate depth scales (calculated from stacking velocities differing by 530 m/sec) are displayed on both sides of the section.

relatively poor source-to-ground couple when the source location was on or near the fault scarp.

To ensure correct identification of reflected events on the stacked section, all coherent arrivals observed on the field plots were visually inspected after each step of the processing flow. The shallowest two reflectors possess distinctively different characteristics than reflectors from deeper in the section. The angle of incidence of these reflectors is greater than the critical angle for each, making them wide-angle reflections. The amplitude and frequency difference observed on these shallow wide-angle reflections resulted from interference with the refracted arrivals. The interference phenomena can most easily be seen on the far traces of the field plots.

The major faulting which produced the present-day scarp can be seen in the subsurface between CDP 295 and CDP 315 (Figure 3). Coherency of reflected energy drops dramatically in this area. Attempting to quantify the observed displacement would be speculative without detailed stratigraphic information.

The reduced amplitude of high-frequency events that appear to be somewhat continuous across the fault can be attributed to horizontal oversampling. Horizontal oversampling results when the subsurface sampled points are closer than the diameter of a Fresnel zone. The diameter (R) of the first Fresnel zone is $R \approx \sqrt{D\,\lambda/2}$, where D is the reflector depth, and λ is the reflected wavelength. The phenomenon seen here (increased frequency and decreased amplitude) results when part of the Fresnel zone around a particular subsurface sampling point begins to extend beyond the fault-related bed truncation. As more of the Fresnel zone passes beyond the bed truncation, the surface area available to reflect energy is reduced; therefore, the amplitude of the returning energy is reduced. The decrease in effective Fresnel zone area in the case of bed truncation also causes the recorded frequency of the reflector to increase slightly. Since the Fresnel zone is large in comparison to the spacing of the subsurface sampling points, the reflector will appear to be thin and extend beyond the actual fault plane.

In addition to the major faulting which produced the scarp, there appears to be faulting on both the upthrown (north) and downthrown (south) portions of the line. However, none of these faults are visible at the surface, suggesting recent inactivity. The upthrown portion of the line is characterized by both gentle folding and faulting deformation. Two parallel reverse slip faults appear to be dipping northward, transecting the seismic section at about CDP 268 and CDP 283, respectively. The lines representing the two parallel faults appear to transect coherent events on the interpreted section. This is a result of oversampling, as discussed above. The downthrown (south) portion of the line is characterized by significantly more coherent reflected events. A reverse slip fault appears to be dipping northward located at approximately CDP 384. The horizontal oversampling remnants again are present in this fault zone.

The approximate depth scales displayed on the sides of the interpreted seismic section were determined using stacking velocities ranging from 1,300 m/sec to 1,830 m/sec (Figure 3).

Conclusions

Presence of the major fault in addition to folding and minor faulting at depths ranging from approximately 30 m to 100 m can be seen on the seismic section (Figure 3). Amplitude, frequency, and wavelet-character changes across individual reflectors helped to delineate deformational features and eventually led to the final interpretation of the shallow structure. The presence of faulting on both flanks of the major fault suggests that the entire Meers fault zone extends at least 180 m in both directions (north and south) from the scarp itself. However, it appears that the only recent deformation has occurred along the localized fault zone associated with the scarp.

Correlation of beds across the major fault zone is conjecture without detailed stratigraphic information such as drill sample or logging data. Therefore, this paper has focused on the shallow structure associated with the Meers fault.

Shallow-seismic reflection has become increasingly popular in the last several years. The

shallow-seismic technique applied in this study presents a fairly detailed picture of the shallow structure. Using this technique in conjunction with stratigraphic information from drilling and wire-line logs could significantly increase the understanding of the structural regime associated with the Meers fault.

Acknowledgments Funding for this research was provided in part by the U. S. Nuclear Regulatory Commission contract no. NRC-04-82-006-02. We appreciate Esther Price's efforts in manuscript preparation and Pat Acker's figure preparations. In addition, we would like to thank Jeff Treadway and Andrew Kalik for their assistance in data acquisition.

References

Brewer, J.A., Study of southern Oklahoma aulacogen, using COCORP deep seismic reflection profiles, Oklahoma Geological Guidebook 21, pp. 31-39, 1982.

Butler, K.R., A structural analysis of the north flank of the Wichita Mountains, Oklahoma, GSA Abs. with Programs, 12, 2, 1980.

Crone, A.J., and Harding, S.T., Relationship of late Quaternary fault scarps to subjacent faults, eastern Great Basin, Utah, Geology, 23, 292-295, 1984.

Crone, A.J., and Luza, K.V., Holocene deformation associated with the Meers fault, southwestern Oklahoma, Oklahoma Geological Guidebook 24, pp. 68-74, 1986.

Donovan, R.N., Sanderson, D.J., and Marchini, D., An analysis of structures resulting from left lateral strike slip movement between the Wichita Mountains and Anadarko basin, southwestern Oklahoma, GSA Abs. with Programs, 14, 476, 1982.

Gilbert, M.C., The Meers fault of southwestern Oklahoma - evidence for possible strong Quaternary seismicity in the Midcontinent [Abs.], EOS, 64, 313, 1983a.

Gilbert, M.C., Timing and chemistry of igneous events associated with the Oklahoma aulacogen, Tectonophysics, 94, 439-455, 1983b.

Hunter, J.A., Pullan, S.E., Burns, R.A., Gagne, R. M., and Good, R.L., Shallow seismic reflection mapping of the overburden-bedrock interface with the engineering seismograph--some simple techniques, Geophysics, 49, 1381-1385, 1984.

Knapp, R.W., and Steeples, D.W., High-resolution common depth point seismic reflection profiling: instrumentation, Geophysics, 51, 276-282, 1986.

Ramelli, A.R., and Slemmons, D. B., Neotectonic activity of the Meers fault, Oklahoma Geological Survey Guidebook 24, pp. 45-54, 1986.

Ramelli, A. R., Slemmons, D.B., and Brocoum, S.J., The Meers fault tectonic activity in southwestern Oklahoma, U. S. Nuclear Regulatory Commission, NUREG ICR-4852, 1-25, A1-A25, 1987.

McLean, R., and Stearns, D.W., Fault analysis in the Wichita Mountains [Abs.], AAPG Bull. 67, 511-512, 1983.

Miller, R.D., Steeples, D.W., Shallow structure from a seismic reflection profile across the Borah Peak, Idaho, fault scarp, Geophysical Research Letters, 12, no. 9, 953-956, 1986.

Slemmons, D.B., Ramelli, A.R., and Brocoum, S.J., Earthquake potential of the Meers fault, Oklahoma, Earthquake Notes, 55, 1, 1985.

Steeples, D.W., Miller, R.D., and Knapp, R.W., 1987, Downhole .50-caliber rifle--an advance in high-resolution seismic sources [Exp. Abs.], in Tech. Prog. Abs. and Biographies, SEG, 57th Ann. Mtg, 1987.

Treadway, J.A., Steeples, D.W., Miller, R.D., Seismic reflections within the upper 100 feet near Borah Peak, Idaho, Earthquake scarp, SEG Exp. Abs., 55th Ann. Internatl. Mtg., pp. 161-163, 1985.

Widess, M. B., How thin is a thin bed?, Geophysics, 38, 1176-1180, 1973.

Paul B. Myers, Richard D. Miller, and Don W. Steeples, Kansas Geological Survey, The University of Kansas, Lawrence, KS 66046.

(Received April 16, 1987;
accepted May 11, 1987.)